



# An efficient motion planning based on grid map: Predicted Trajectory Approach with global path guiding

Sen Han, Lei Wang, Yiting Wang\*, Huacheng He

State Key Laboratory of Ocean Engineering, Shanghai Jiao Tong University, Shanghai 200240, China  
SJTU-Sanya Yazhou Bay Institute of Deepsea Science and Technology, Sanya 572024, China

## ARTICLE INFO

**Keywords:**

Unmanned surface vehicle (USV)  
Motion planning  
Predicted trajectory approach  
Collision avoidance

## ABSTRACT

This paper presents a Predicted Trajectory Approach (PTA) for global motion planning of an underactuated unmanned surface vehicle (USV). Different from the conventional path planning algorithms which mostly focus on the shortest, safest or smoothest paths, PTA takes all the dynamic constraints of the USV into account, and finds the global trajectory that can be traced precisely via its own maneuvering system. In present strategy, the predicted trajectories produced by the mathematical model of the USV are decomposed into a series of waypoints on grid map. Then an efficient trajectory can be found for the USV by performing the A\* search method. To improve the search efficiency and accuracy, the PTA is enhanced with global path guiding (GPTA). When searching for feasible trajectories, GPTA can employ the global path obtained by Theta\* to accurately estimate the heuristic cost of the objective function, rather than using the Euclidean distance directly as PTA does. Numerical simulations in various scenarios are conducted to compare the performance of the PTA, GPTA, Trajectory Units (TUs) and hybrid path planning algorithm combining global and local path planning (HGL). The results demonstrate that GPTA has higher safety and navigation efficiency for motion planning of the underactuated USV.

## 1. Introduction

Due to the continuous demand for exploring oceanic resources, unmanned surface vehicles (USVs) have been increasingly applied in both commercial and military fields, including ocean sampling, environmental monitoring, bathymetric survey, maritime search and rescue, hydrologic survey, harbor surveillance, and defense (Svec and Gupta, 2012; Sharma et al., 2014; Liu and Bucknall, 2016). To autonomously execute these sophisticated tasks, it is vital to plan out a high-efficiency trajectory for an USV. However, finding a practical trajectory becomes rather challenging since the feasibility, safety, and efficiency are compositely required to be optimized in complicated marine environments including static obstacles, dynamic obstacles and environmental perturbations (Claussmann et al., 2020; Wang et al., 2020). Path planning, as one of the critical technologies of USV navigation, has been drawing much attention. According to different dynamic constraints, the path planning can be divided into three stages: route planning, trajectory planning and motion planning (Gu et al., 2020; Zhou et al., 2020b). Dynamic constraints (Zhou et al., 2020b) are defined as the restrictions on the ship's motion (including position, velocity and acceleration) due to its physical limitations (e.g. maximum, minimum and change rate of surge force provided by propeller).

Route planning regards the USV as a particle and ignores all dynamic constraints. Song et al. (2019) proposed a smoothed A\* algorithm for route planning of unmanned surface vehicles. Compared to the conventional A\* algorithm, the proposed approach retained the fast and efficient route searching and made it more suitable for USV navigation. Shah and Gupta (2016, 2019) presented the speeding up A\* on Visibility Graphs method to search long distance paths in large size of the marine environment. To improve search efficiency, the focused search algorithm and the associated search heuristics were developed to reduce the computational time without significantly sacrificing the optimality of the computed path. However, it is inevitable that the computational time of the developed algorithm will increase with the growing obstacle density. Wu et al. (2021) proposed a long-distance route planning method based on multi-scale Visibility Graph to solve the problems of the slow planning and poor route accuracy. In these researches, the application scenarios of route planning mainly concentrate on large-scale environments. But for the USV performing in complex terrains, such as the harbor and inland river, route planning is difficult to be directly applied.

Most USVs are underactuated, and their motion is restricted by nonholonomic kinematic constraints and the limited control authority

\* Corresponding author at: State Key Laboratory of Ocean Engineering, Shanghai Jiao Tong University, Shanghai 200240, China.  
E-mail address: [zjgwangyiting@sjtu.edu.cn](mailto:zjgwangyiting@sjtu.edu.cn) (Y. Wang).

of real actuators. To ensure that a USV can trace the planned trajectory with minimal errors, and thus help to guarantee collision-free operation, the trajectories generated by the planner should account for the inherent limitations of the vehicle's dynamic response (Bertaska et al., 2015; Shah et al., 2016; Bertaska and von Ellenrieder, 2019). Trajectory planning considers partial dynamic constraints, like size, speed, heading and curvature (Chrpa and Osborne, 2014; Du et al., 2019). Kim et al. (2014) and Lee et al. (2015) suggested a new angular rate-constrained Theta\* (ARC-Theta\*) algorithm in which the planned paths considered the constraints of both yaw rates and heading angles of the USV. Liu et al. (2017) developed an angle-guidance fast marching square algorithm, which was able to search the optimal path based on USV's motion constraints. Chen et al. (2020) proposed a hybrid approach of fast marching square and velocity obstacles method for global path planning with consideration of both velocity constraint of the ship and influences of collision risk. All these methods had found feasible trajectories and achieved good results. However, some interactions among the constraints might be ignored in these trajectory planning approaches (Zhou et al., 2020b).

Motion planning considers the overall dynamic constraints. Pettit and Fraichard (2005) presented a variant of the rapidly exploring random tree (RRT) algorithm to obtain feasible trajectories in high dimensional state spaces for robots with dynamical constraints. However, the planned trajectories are generally rough due to the use of random sampling during the search. The problem was solved by a newly developed variant of the algorithm named RRT\* (Karaman and Frazzoli, 2010). Approaches based on Random Sampling are widely used in motion planning of the robotics, such as industrial robots, unmanned ground vehicle, unmanned aerial vehicle, etc (Moon and Chung, 2015; Salzman and Halperin, 2016; Li et al., 2018). However, the large inertia, resistance and response time of the USV may introduce difficulties when applying the approach, apart from the complicated interference of wind, wave and current (Fossen et al., 2017; Zhang et al., 2015). Thus, the above methods on Random Sampling need to be further improved for USV's motion planning (Zhou et al., 2020b). Moreover, the search-based deliberative motion planning approach had also been widely used (Likhachev and Ferguson, 2009; Dolgov et al., 2010; Bertaska et al., 2013; Švec et al., 2013; Švec et al., 2014). The challenge of this approach is that the computational time significantly increases with the increase in the dimension of the state space, complexity of the motion primitive set, complexity of the environment, etc.

As for the motion planning of USVs, Du et al. (2018) proposed a Trajectory Units approach to realize the fine motion control in a small range of scenario. However, most trajectories from their search approach were not smooth under the influence of obstacles and its computational time increased exponentially with the expanded search area. Zhou et al. (2020a) further gave a novel motion-planning method based on topological position relationships (TPR) for dealing with the long-search-time problem and making the planned trajectory more realistic. Yoo and Kim (2016) adopted the reinforcement learning algorithm to produce feasible trajectories considering the dynamic characteristics of the vehicle and ocean disturbances. Moreover, some researchers proposed several hybrid algorithms that effectively combining global and local path planning to deal with the motion planning problem (Wang et al., 2018; Chen et al., 2019; Wang and Xu, 2020). These hybrid algorithms can be divided into two steps: First, an unblocked initial path from the starting point to the goal can be acquired by means of a traditional global route planning algorithm, such as A\* (Shi et al., 2019), Theta\* (Daniel et al., 2010), Fast Marching Method (Wang et al., 2019), etc; second, the local planning approach is employed to produce the final trajectory which contains kinematics and dynamics constraints of USVs. These hybrid path planning algorithms have good real-time performance and strong dynamic obstacle avoidance capability. However, the hybrid scheme can only guarantee the optimality of the global path. The trajectory obtained by local quadratic planning is just the fitting result of the global path and

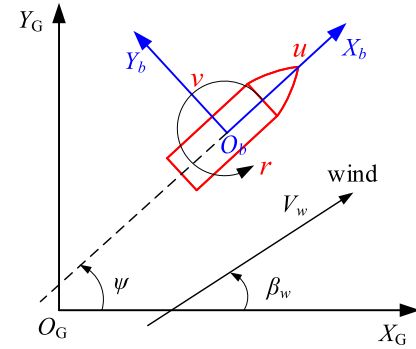


Fig. 1. The coordinate systems of USV motion.

cannot be proved to be optimal. Therefore, how to directly find an efficient trajectory through a global motion planning approach is an open problem.

In present paper, we propose a Predicted Trajectory Approach with global path guiding (GPTA) to perform the global motion planning for USVs. Considering all dynamic constraints of the USV, the approach combines the predicted trajectories with grid map, and employs the A\* search method to find the efficient trajectory. To improve the computational efficiency, the Theta\* is used to generate the global shortest path which can accurately estimate the heuristic cost of the objective function.

The rest of present paper is organized as follows: Section 2 briefly describes the mathematical model for USVs motion under environmental perturbations. In Section 3, the PTA and GPTA are proposed to carry out the motion planning for an underactuated USV. Simulation results are presented and discussed in Section 4 considering the algorithmic comparison and environmental influence. Section 5 gives concluding remarks concerning our works.

## 2. Mathematical model of the USV

The horizontal motions and control variables of USV are defined and measured with respect to the north-up coordinate system  $\{n\}$  and the body-fixed coordinate system  $\{b\}$ , as shown in Fig. 1. The north-up coordinate system is denoted as  $X_G O_G Y_G$  frame, in which the position and orientation of USV are measured relative to a defined origin. The body-fixed coordinate system  $X_b O_b Y_b$  is fixed to the USV and moves along with it.

Horizontal motion responses of the USV, including surge, sway and yaw, have dynamics resulting from the propeller, rudder and environmental loads. The relationship between the generalized position in  $\{n\}$  and generalized velocity in  $\{b\}$  is given through a transformation matrix  $R(\psi)$

$$\dot{\eta} = R(\psi)v \quad (1)$$

where  $R(\psi)$  is

$$R(\psi) = \begin{bmatrix} \cos(\psi) & -\sin(\psi) & 0 \\ \sin(\psi) & \cos(\psi) & 0 \\ 0 & 0 & 1 \end{bmatrix} \quad (2)$$

To simulate the motion responses under environmental forces and control efforts, the generalized three degrees of freedom equations that ignore the roll, pitch and heave motions are used as follows (Fossen, 2011):

$$M_{RB}\ddot{v} + M_A\ddot{v}_r + C_{RB}(v)v + C_A(v_r)v_r + D(v_r)v_r = \tau + \tau_{wind} \quad (3)$$

where  $M_{RB}$  is the rigid-body inertia matrix.  $M_A$  is the hydrodynamic added mass.  $C_{RB}(v)$  is the matrix of rigid-body Coriolis and centripetal forces.  $C_A(v_r)$  is the corresponding Coriolis and centripetal matrix due

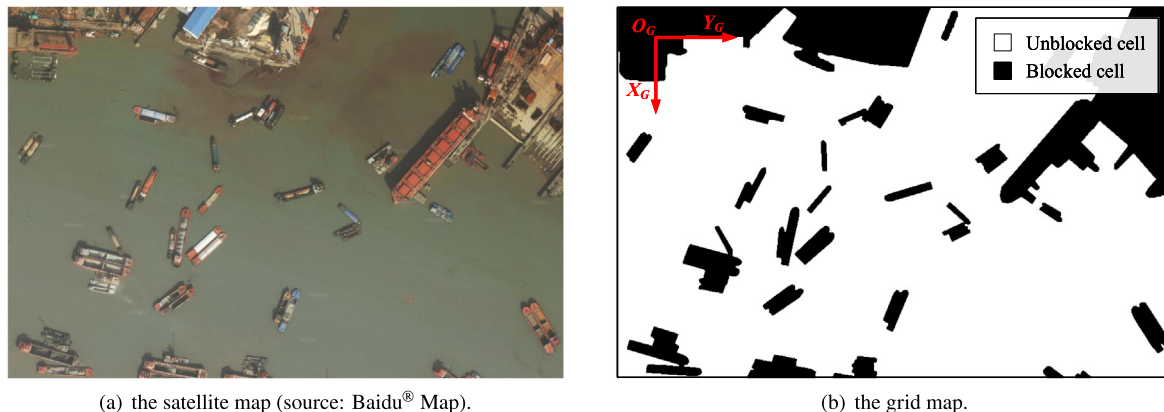


Fig. 2. Conversion from the satellite image to grid map.

to added mass.  $\mathbf{D}(\mathbf{v}_r)$  is the damping matrix.  $\boldsymbol{\eta} = [x, y, \psi]^T$  is the generalized position vector of the USV, corresponding to the  $X_G$ -axis position,  $Y_G$ -axis position and yaw angle, respectively.  $\mathbf{v} = [u, v, r]^T$  is the vector of generalized velocity, denoting the surge velocity, sway velocity and yaw rate of the vehicle, respectively.  $\mathbf{v}_r = \mathbf{v} - \mathbf{v}_c$  is the relative velocity vector and  $\mathbf{v}_c$  is the generalized ocean current velocity of an irrotational fluid.  $\boldsymbol{\tau} = [\tau_u, \tau_v, \tau_r]^T$  denotes the vector of control forces, including surge force, sway force and yaw moment.  $\boldsymbol{\tau}_{\text{wind}}$  is the wind loads.

The relevant vectors in Eq. (3) are expressed as

$$\mathbf{M}_{RB} = \begin{bmatrix} m & 0 & 0 \\ 0 & m & mx_g \\ 0 & mx_g & I_z \end{bmatrix}, \quad \mathbf{M}_A = \begin{bmatrix} -X_{\dot{u}} & 0 & 0 \\ 0 & -Y_{\dot{v}} & -Y_{\dot{r}} \\ 0 & -N_{\dot{v}} & -N_{\dot{r}} \end{bmatrix} \quad (4)$$

$$\mathbf{C}_{RB}(\mathbf{v}) = \begin{bmatrix} 0 & 0 & -m(x_g r + v) \\ 0 & 0 & mu \\ m(x_g r + v) & -mu & 0 \end{bmatrix} \quad (5)$$

$$\mathbf{C}_A(\mathbf{v}_r) = \begin{bmatrix} 0 & 0 & Y_{\dot{v}} v_r + 0.5(N_{\dot{v}} + Y_{\dot{r}})r \\ 0 & 0 & -X_{\dot{u}} u_r \\ -Y_{\dot{v}} v_r - 0.5(N_{\dot{v}} + Y_{\dot{r}})r & X_{\dot{u}} u_r & 0 \end{bmatrix} \quad (6)$$

where  $m$  is the mass of the ship and  $I_z$  is the moment of inertia about the yaw rotation. The hydrodynamic coefficients  $X_{(\cdot)}, Y_{(\cdot)}, N_{(\cdot)}$  represent hydrodynamic derivatives because they are the partial derivatives of the forces and moment with respect to the corresponding velocities, e.g.  $Y_r$  is the drag coefficient in the  $Y$  direction due to angular velocity in the direction of  $r$  (See Box I).

The wind loads acting on USVs are computed as follows:

$$\boldsymbol{\tau}_{\text{wind}} = \begin{bmatrix} X_{\text{wind}} \\ Y_{\text{wind}} \\ N_{\text{wind}} \end{bmatrix} = \frac{1}{2} \rho_a V_{rw}^2 \begin{bmatrix} C_X(\gamma_{rw}) A_{Fw} \\ C_Y(\gamma_{rw}) A_{Lw} \\ C_N(\gamma_{rw}) A_{Lw} L_{oa} \end{bmatrix} \quad (8)$$

where  $X_{\text{wind}}, Y_{\text{wind}}$  and  $N_{\text{wind}}$  are longitudinal and lateral forces, and yaw moment acting on the hull.  $\rho_a$  is the air density.  $C_X, C_Y$  and  $C_N$  are the wind coefficients for horizontal plane motions.  $A_{Fw}$  and  $A_{Lw}$  are frontal and lateral projected area respectively.  $L_{oa}$  is the length overall of ship.  $V_{rw}$  is the relative wind speed and  $\gamma_{rw}$  is the wind angle of attack relative to the bow, which can be expressed by:

$$V_{rw} = \sqrt{u_{rw}^2 + v_{rw}^2} \quad (9)$$

$$\gamma_{rw} = -\text{atan}2(v_{rw}, u_{rw}) \quad (10)$$

The relative velocities are

$$u_{rw} = u - u_w \quad (11)$$

$$v_{rw} = v - v_w \quad (12)$$

The components of  $V_w$  in the  $X_b$  and  $Y_b$  directions are

$$u_w = V_w \cos(\beta_w - \psi) \quad (13)$$

$$v_w = V_w \sin(\beta_w - \psi) \quad (14)$$

where  $V_w$  is the wind speed and  $\beta_w$  is the wind direction.

For a fully actuated system, motion planning is unnecessary because the ship can trace most trajectories by adjusting and optimizing the control parameters. However, not all motion states can be satisfied for an underactuated system where the degrees of control are less than the degrees of freedom. Considering that most ships are underactuated equipped with limited propeller and rudder, present paper focuses on underactuated USVs, using motion planning approach to find an efficient trajectory from the starting point to the goal.

In order to simplify the model, the surge force is assumed to be a constant. Considering that the sway force acting on the underactuated USVs is relatively small, the sway force is assumed to be zero. Only the yaw moment is directly applied as the control input of the ship's mathematical model.

### 3. Global motion planning

#### 3.1. Environmental mapping based on grid map

A global map containing environmental information is firstly established. Grid Map, as one of the most widely used methods in robotics and video games (Lee et al., 2011; Nash and Koenig, 2013), decomposes a satellite map into grids with blocked and unblocked cells. Each pixel in the satellite map is identified as either 1 or 0 by means of a binarization function, "im2bw" in MATLAB. Thus, the satellite map is converted to a binary array and conveniently stored in computers. Fig. 2 shows an anchorage in the Yangtze River and its grid map after rasterization.

To ensure the navigation safety of the USV, the original grid map needs to be expanded with obstacles (Niu et al., 2018, 2020). In the strategy, each blocked cell is expanded by  $S_r$  meters, as shown in Fig. 3.

The expanded cells will be treated as the blocked cells for motion planning. Therefore, only the trajectory that avoids all expanded cells can be viewed as a successful obstacle avoidance. In this way, the USV can travel safely.

In addition, the safe grid map method (Zhong et al., 2020) is also used to evaluate the risk costs of unblocked cells located near the expanded cells. The following risk function  $R(c)$  can be defined as

$$R(c) = \begin{cases} 5 & d \leq S_1 \\ 4 & S_1 < d \leq S_2 \\ 3 & S_2 < d \leq S_3 \\ 2 & S_3 < d \leq S_4 \\ 1 & d > S_4 \end{cases} \quad (15)$$

$$\mathbf{D}(\mathbf{v}_r) = \begin{bmatrix} -X_u - X_{|u|u}|u_r| - X_{uuu}u_r^2 & 0 & 0 \\ 0 & -Y_v - Y_{|v|v}|v_r| - Y_{|r|v}|r| & -Y_r - Y_{|v|r}|v_r| - Y_{|r|r}|r| \\ 0 & -N_v - N_{|v|v}|v_r| - N_{|r|v}|r| & -N_r - N_{|v|r}|v_r| - N_{|r|r}|r| \end{bmatrix} \quad (7)$$

Box I.

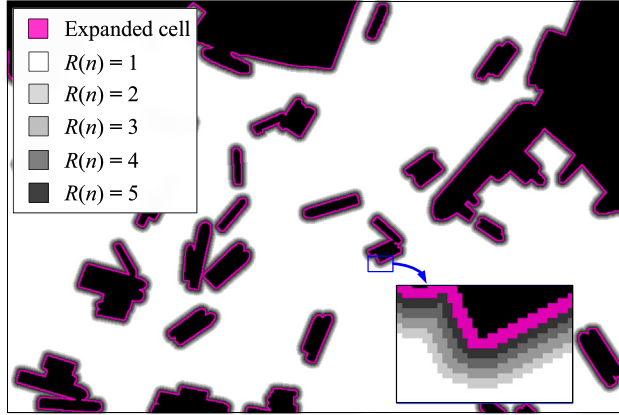


Fig. 3. The safe grid map.

where  $d$  represents the distance between the unblocked cell and its nearest expanded cell.  $S_1$ ,  $S_2$ ,  $S_3$  and  $S_4$  are the threshold values of distance.

The risk costs of all unblocked cells is evaluated by  $R(c)$  to obtain the safe grid map with risk areas, as shown in Fig. 3. A layer of risk cells with decreasing gray values is produced near expanded cells.

### 3.2. PTA on grid map

Taking the physical characteristics of propeller and rudder into account, PTA firstly obtains two sets: the dynamic window  $M_d$  and the feasible region  $M_f$ .  $M_d$  contains all the yaw moments the USV can achieve within the unit sampling interval  $\Delta T$ . Based on the current yaw moment, the dynamic window is defined as

$$M_d = \{\tau_r \in R | \tau_r \in [\tau_{rc} - \dot{\tau}_r \cdot \Delta T, \tau_{rc} + \dot{\tau}_r \cdot \Delta T]\} \quad (16)$$

where  $\tau_{rc}$  is current control input of yaw moment, and  $\dot{\tau}_r$  is the maximum differential of yaw moment.

Determined by the USV's inherent properties, the feasible region can be expressed as

$$M_f = \{\tau_r \in R | \tau_r \in [\tau_{r\min}, \tau_{r\max}]\} \quad (17)$$

Considering the two limitations, the moment space  $M_s$  is defined by their intersection

$$M_s = M_d \cap M_f \quad (18)$$

Then, the moment space is discretized into a series of feasible yaw moments according to a given interval  $\Delta\tau_r$ . For each feasible yaw moment, the trajectory can be predicted by using mathematical model of the USV (Han et al., 2021), as shown in Fig. 4. During the whole process, the USV travels forward within the predicted time  $T_p$ , and the feasible yaw moment maintains unchanged.

Finally, all predicted trajectories are decomposed into waypoints according to the unit sampling interval  $\Delta T$ . If a waypoint is located in the blocked cells (the blue dotted line in Fig. 4) or two adjacent waypoints are blocked (the red dotted line in Fig. 4), the corresponding trajectory will be discarded. The *LineOfSight* function (Daniel et al., 2010) is used to determine whether there is an obstacle between two waypoints in grid map.

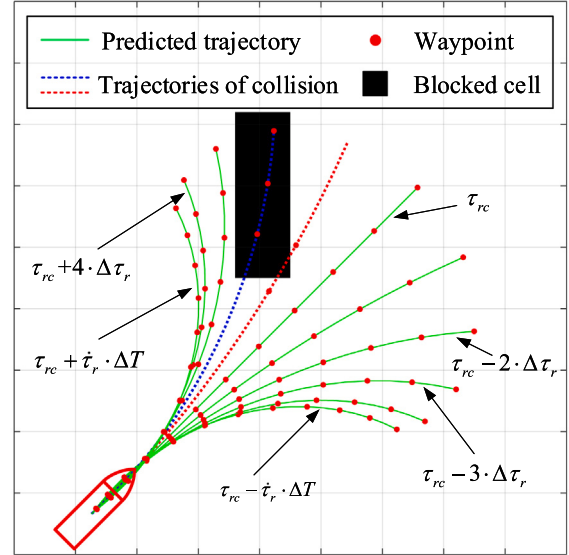


Fig. 4. The schematic diagram of predicted trajectories and decomposed waypoints.

### 3.3. Waypoint chosen by A\* search

Similar to the application of A\* on Visibility Graphs (Lozano-Pérez and Wesley, 1979), A\* search method can also be used for finding the feasible waypoints on grid map. Considering the risk costs of cells in grid map, the objective function of the traditional A\* algorithm in present paper is updated as

$$F(c) = G(c) + H(c) + \lambda \cdot \sum R(c) \quad (19)$$

where the g-value  $G(c)$  is the actual time cost from the starting point to the waypoint found so far. The user-provided h-value  $H(c)$  is the heuristic cost from the waypoint to the goal.  $\sum R(c)$  is the accumulated risk value from the starting point to the waypoint according to Eq. (15).  $\lambda$  is the safety weighting coefficient. The f-value  $F(c)$  is an estimate sailing time corresponding to the trajectory from the starting point via the waypoint to the goal.

When using the A\* search method, the performance of final trajectory may deteriorate if the estimated cost of h-value is greater than its actual cost (Hart et al., 1968). Therefore,  $H(c)$  can be expressed as

$$H(c) = \frac{L_d}{V_{\max}} \quad (20)$$

where  $L_d$  is the Euclidean distance between the waypoint and the goal,  $V_{\max}$  represents the maximum speed USV can achieve.

In addition, A\* search method maintains two global data structures:

- (1) The open list is a priority queue containing the cells that A\* considers for expansion;
- (2) The closed list is a set containing all cells that A\* has already been expanded. It ensures that A\* expands each cell at most once.

Fig. 5 shows an example trace of PTA.

Iteration 0: The coordinate of the starting point is L1 (green triangle), and the goal is A12 (green pentagram). At the starting point, the

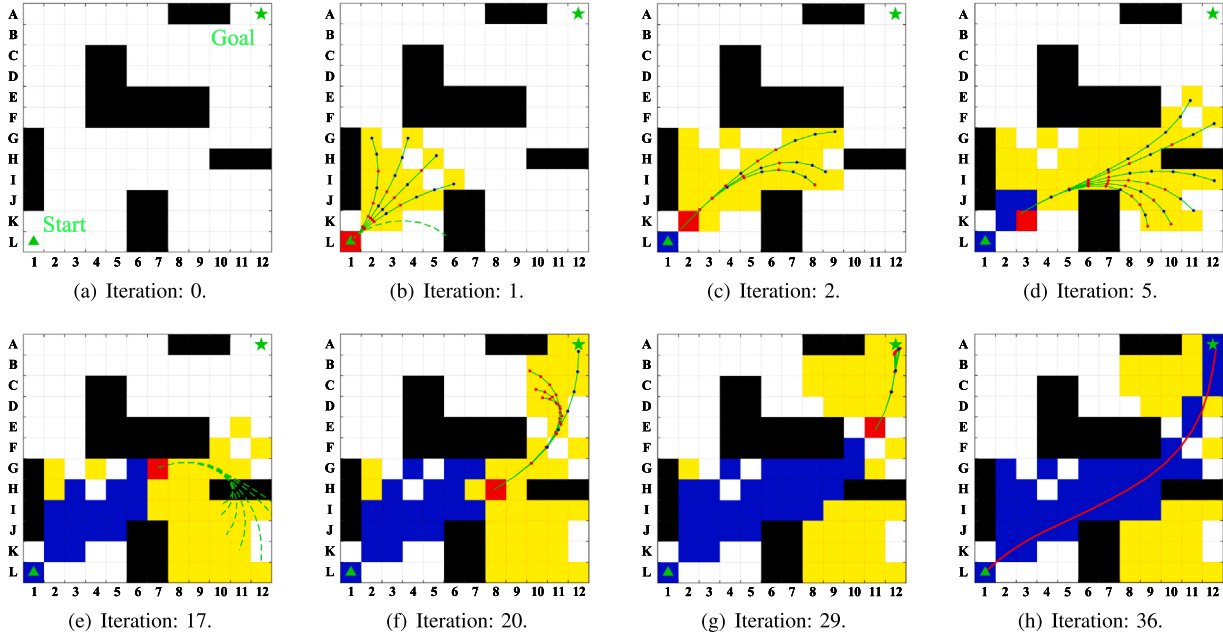


Fig. 5. Example trace of PTA.

initial motion states of USV (including position information and speed information) and current control input of yaw moment are given.

Iteration 1: The starting point is selected as the current waypoint (CWP). According to Eq. (16)–(18), the moment space is obtained. And the trajectories can be predicted by putting the discrete yaw moment into the mathematical model of USV. If the predicted trajectory collides with the obstacle or boundary, it will be discarded (the green dotted trajectory in Fig. 5(b)). The remaining trajectories will be decomposed into waypoints, and the f-value of each waypoint is calculated according to Eq. (19). If there are multiple waypoints in the same cell like K2, the waypoint with the smallest f-value will be selected and added to the open list (the waypoint turns blue and the cell corresponding to the waypoint turns yellow), so as to realize one-to-one matching between the waypoint and the cell. At the same time, the motion information and control input arriving at this waypoint are saved in the corresponding cell, so as to retrieve the feasible trajectory from the CWP to the starting point in reverse. Finally, the CWP adds to the close list (the cell corresponding to the CWP will turn blue in the next iteration). The flow chart of search process is shown in Fig. 6.

Iteration 2: The waypoint with the smallest f-value in open list is taken as the new CWP. Taking the motion states and yaw moment of new CWP as the input of USV model, the predicted trajectories can be generated. In this way, the initial and final states of each trajectory are continuous. Then, the newly expanded waypoint and its f-value can also be obtained through the flow chart as can be observed in Fig. 6. If the f-value of the newly obtained waypoint is smaller than the old value of its corresponding cell in open list, the old one will be replaced by the newly expanded waypoint to keep the one-to-one matching between the cell and the waypoint. The motion information and control input stored in the corresponding cell are also be updated. For example, the f-value of the newly expanded waypoint in cell I6 of Iteration 2 is smaller than that of Iteration 1, so the waypoint stored in cell I6 of open list needs to be replaced by the newly expanded waypoint.

Iteration 5: It can be seen that several newly generated trajectories can bypass obstacles and gradually approach to the goal.

Iteration 17: All predicted trajectories collide with the obstacles or exceed the boundary. It means that no waypoints are generated in this iteration and the open list is not updated. Then PTA need to determine whether the open list is empty according to the flow chart in Fig. 6. If the open list is empty, the motion planning fails and no

feasible trajectory can be found. If not, the waypoint with the smallest f-value from open list will be chosen as the new CWP and the iteration continues.

Iteration 20: A new expanded waypoint appears on the cell where the goal is located, indicating that the algorithm has found a feasible trajectory from the starting point to the goal. But this trajectory may not be optimal.

Iteration 29: Waypoint in the goal cell A12 have been updated, indicating that the search algorithm has found a more efficient trajectory.

Iteration 36: When the CWP is located at the goal cell, the final trajectory can be reconstructed inversely according to the motion states of waypoints saved in cells previously.

### 3.4. PTA with global path guiding

As a heuristic cost, the larger the h-value is, the higher the searching efficiency of the algorithm will be. However, the estimated cost of h-value should be less than its actual cost to ensure the performance of the final trajectory found by A\* search method (Hart et al., 1968; Lozano-Pérez and Wesley, 1979). PTA directly uses the Euclidean distance to calculate the sailing time from the waypoint to the goal, while the true shortest distance between them is always greater than the Euclidean distance. As shown in Fig. 7, when the h-value of waypoint C in cell H5 is calculated, PTA will directly use the straight-line distance C-A12 to estimate the sailing time of USV. But the path C-A12 does not represent the true shortest path taking the obstacle into account. Therefore, using Euclidean distance to estimate the sailing time from waypoint to the goal may lead to the decrease of search efficiency.

Different from the PTA, this paper also proposed an PTA with global path guiding (GPTA) to improve the search efficiency. GPTA obtains a global shortest path from the starting point to the goal before the algorithm runs. The solid blue line L1-P-A12 in Fig. 7 is the true shortest path from the starting point to the goal using Theta\* algorithm (Nash and Koenig, 2013). When calculating the true shortest distance, the GPTA needs to find a visible turning point closest to the waypoint. For example, P is the visible turning point that the waypoint C needs to seek in Fig. 7, so the true shortest distance from the waypoint C to the goal is the path C-P-A12. It should be noted that the LineOfSight

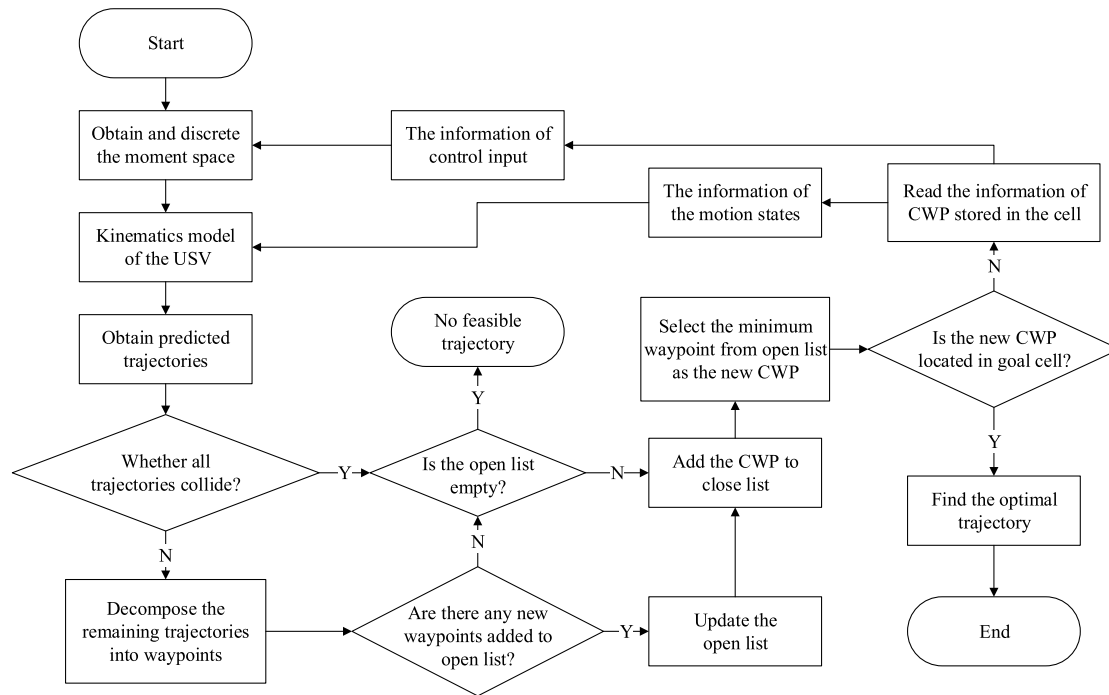


Fig. 6. The flow chart of the algorithm.

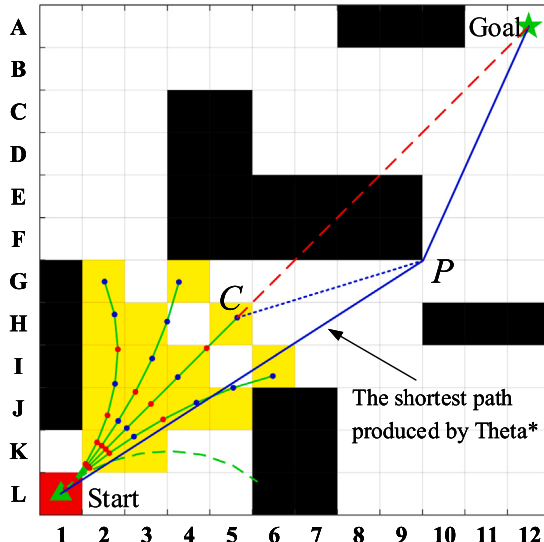


Fig. 7. Schematic diagram of global path guiding.

function (Daniel et al., 2010) is used to judge whether two points are visible. Therefore, the calculation of h-value in GPTA is changed to

$$H(c) = \frac{L_{\text{shortest}}}{V_{\max}} \quad (21)$$

where  $L_{\text{shortest}}$  represents the true shortest distance from the waypoint to the goal.

#### 4. Results and discussion

In this section, multiple simulation experiments with different methods and environmental perturbations are implemented to verify the proposed motion planning approaches. Considering the underactuated characteristic of USV, CyberShip II (Skjetne et al., 2004) is used in

**Table 1**  
Simulation parameters.

Description	Notations	Value
Unit sampling time (s)	$\Delta T$	0.5
Predicted time (s)	$T_p$	5
Maximum speed of USV (m/s)	$V_{\max}$	0.581
Interval of yaw moment (N m)	$\Delta \tau_r$	0.15
Maximum values of yaw moment (N m)	$\tau_{r,\max}$	1.5
Minimum values of yaw moment (N m)	$\tau_{r,\min}$	-1.5
Surge force (N)	$\tau_u$	2
Derivative of yaw moment (N· m/s)	$\dot{\tau}_r$	0.6
Distance of obstacle expanding (m)	$S_r$	0.3
$S_1$	$S_1$	0.2
$S_2$	$S_2$	0.4
The threshold values of distance (m)	$S_3$	0.6
$S_4$	$S_4$	0.8

present paper by ignoring the redundant propulsion and steering device. Its mass is 23.8 kg, length is 1.255 m, and breadth is 0.29 m. The map in Fig. 2(b) is consist of  $900 \times 600$  grids and the length of each grid is 0.1 m. Other simulation parameters are shown in Table 1. All path-planning algorithms are implemented in MATLAB 2018b and executed on Intel Core 9 CPU 3.6 GHz with 32 GB RAM.

#### 4.1. Comparative studies

In present subsection, the initial generalized position of the USV is  $\eta_0 = [22, 76, \pi/4]^T$ , the initial generalized velocity is  $v_0 = [0, 0, 0]^T$ , and the goal is  $\eta_g = [50, 20]^T$ .

##### 4.1.1. Comparisons of PTA and GPTA

The biggest difference between PTA and GPTA is that the h-value used by PTA is the Euclidean distance, while GPTA uses the true shortest distance obtained by Theta\* algorithm. Numerical simulations separately based on PTA and GPTA are conducted and the results of planned trajectories and expanded cells are shown in Fig. 8.

It can be seen from Fig. 8 that the planned trajectories of both PTA and GPTA are smooth and none of them collide with obstacles. For an intuitive comparison, the performances of PTA and GPTA are

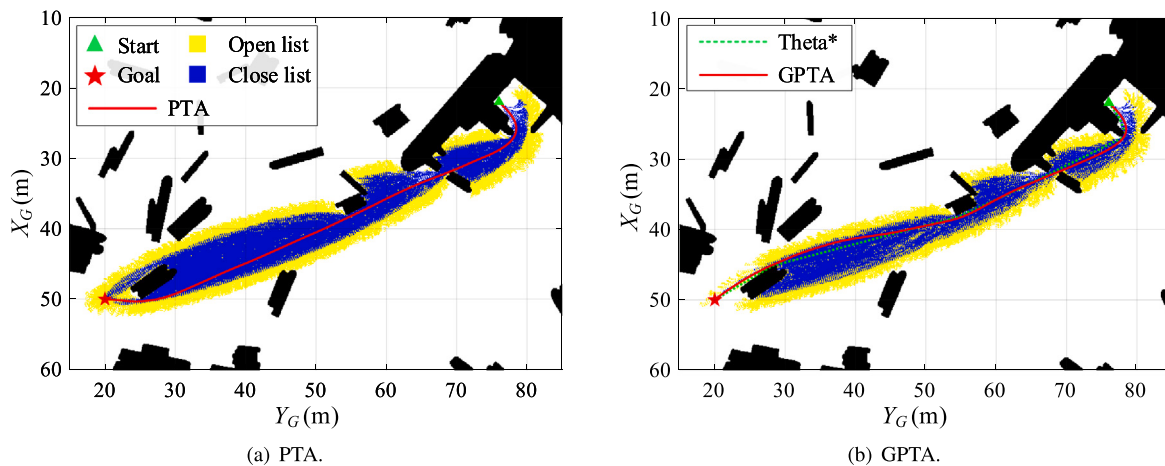


**Fig. 8.** The results of planned trajectories and expanded cells.

**Table 2**  
Performances of PTA and GPTA.

Methods	Cells added to open list	Cells in close list	Computational time (s)	Trajectory length (m)	Sailing time (s)	Heading change (rad)
PTA	175314	27174	25.65	69.24	126.5	4.75
GPTA	139206	19261	19.13	68.62	125.5	4.66

summarized in [Table 2](#). The trajectory length and sailing time refer to the total length and efficiency of the USV's navigation from the starting point to the goal, respectively. Heading change is the sum of yaw velocities during the whole voyage. The computational time is an average value of 1000 runs. According to the statistics, GPTA has better performance in terms of both computational efficiency and navigation efficiency compared to PTA.

Different from the local planning, GPTA is a global motion planning approach which does not perform real-time reactions to uncertain obstacles. Accordingly, it may take a long time to find the efficient trajectory in an intricate mapped environment. Considering the feature of offline computing, the computational efficiency of GPTA will be ignored in the following analysis.

#### 4.1.2. Comparisons of TUs, HGL and GPTA

To validate the proposed approach, the Trajectory Units (TUs) proposed by [Du et al. \(2018\)](#) and hybrid algorithm combining global and local path planning (HGL) proposed by [Wang and Xu \(2020\)](#) are carried out to compare their performances of motion planning. [Fig. 9](#) shows the results of planned trajectories, motion states (including yaw angles, surge and sway velocities) and yaw moments.

As can be seen from [Fig. 9\(a\)](#), trajectories obtained by HGL and GPTA are significantly better than TUs. In terms of sailing time, USV needs 125.5 s to reach the goal with the trajectory obtained by HGL, while GPTA needs 125 s. In [Fig. 9\(b\)](#), the yaw moment of HGL fluctuates greatly during steering. Frequent adjustment of rudder is not only harmful for navigation safety, but also increases wear of mechanism devices. Inversely, the yaw moments of both TUs and GPTA maintain relatively stable.

#### 4.1.3. Comparisons of TUs, HGL and GPTA on expanded grid map

As the grid map expands, some areas may become too narrow for the USV to pass through. In present subsection, TUs, HGL and GPTA are performed on expanded grid map, as can be observed in [Fig. 10](#).

After expanding the obstacles, TUs and GPTA take 144.5 s and 129 s respectively for the whole voyage. And HGL fails to plan at 33.5 s and no feasible trajectory is found, as shown in [Fig. 10](#). The core of HGL is to use global path to guide local planning. In narrow waters, the global planning method can still avoid obstacles to find the shortest

path. Whereas, the local planning is easy to fall into local extremum caused by the inflection points of large curvature in the global path, which exceed the performance of USV and result in planning-failure.

#### 4.1.4. Comparisons of GPTA with different safety weighting coefficients

In order to avoid the USV being too close to obstacles, the safe grid map is created to evaluate the risk costs of cells. GPTA with different safety weighting coefficients is performed to compare their performances of motion planning. The results of planned trajectories, motion states and yaw moments are shown in [Fig. 11](#).

As shown in [Fig. 11\(a\)](#), a layer of risk cells with decreasing gray values will be produced near expanded cells, which is marked as the dangerous areas. When the weight is 0.02, the planned trajectory directly passes through the dangerous areas and sails out of the dock, while the USV will first choose to turn left to stay away from the dangerous areas when the weight is 0.05 or 0.08. This difference can also be seen from the yaw angle in the first 10 s of [Fig. 11\(b\)](#). When the weights are 0.02, 0.05, 0.08, the sailing times from the starting point to the goal are 129 s, 132 s and 133 s, and the accumulated risk values  $\sum R(c)$  are 178, 91 and 78, respectively. Increasing of the safety weighting coefficient, the planned trajectory will be far away from the obstacles, and the sailing time of the ship will be longer. Considering the combination of the navigation efficiency and safety,  $\lambda = 0.05$  is selected in the following simulations.

#### 4.2. Motion planning under wind and current perturbations

In present subsection, the influence of environmental loads including wind and current is discussed for global motion planning.

##### 4.2.1. The influence of wind

The initial generalized position of the USV is  $\eta_0 = [16, 72, -3\pi/4]^T$ , the initial generalized velocity is  $v_0 = [0, 0, 0]^T$ , and the goal is  $\eta_g = [33, 10]^T$ . When the wind direction is  $\beta_w = -3\pi/4$ , the planned trajectories, motion states and yaw moments obtained by using the GPTA under different wind speeds are shown in [Fig. 12](#).

When the wind speeds are 0.5 m/s, 1.5 m/s and 2.5 m/s, the USV needs 119 s, 118 s and 116.5 s for arrival, respectively. Therefore, the current wind direction is favorable to the USV's navigation. In terms

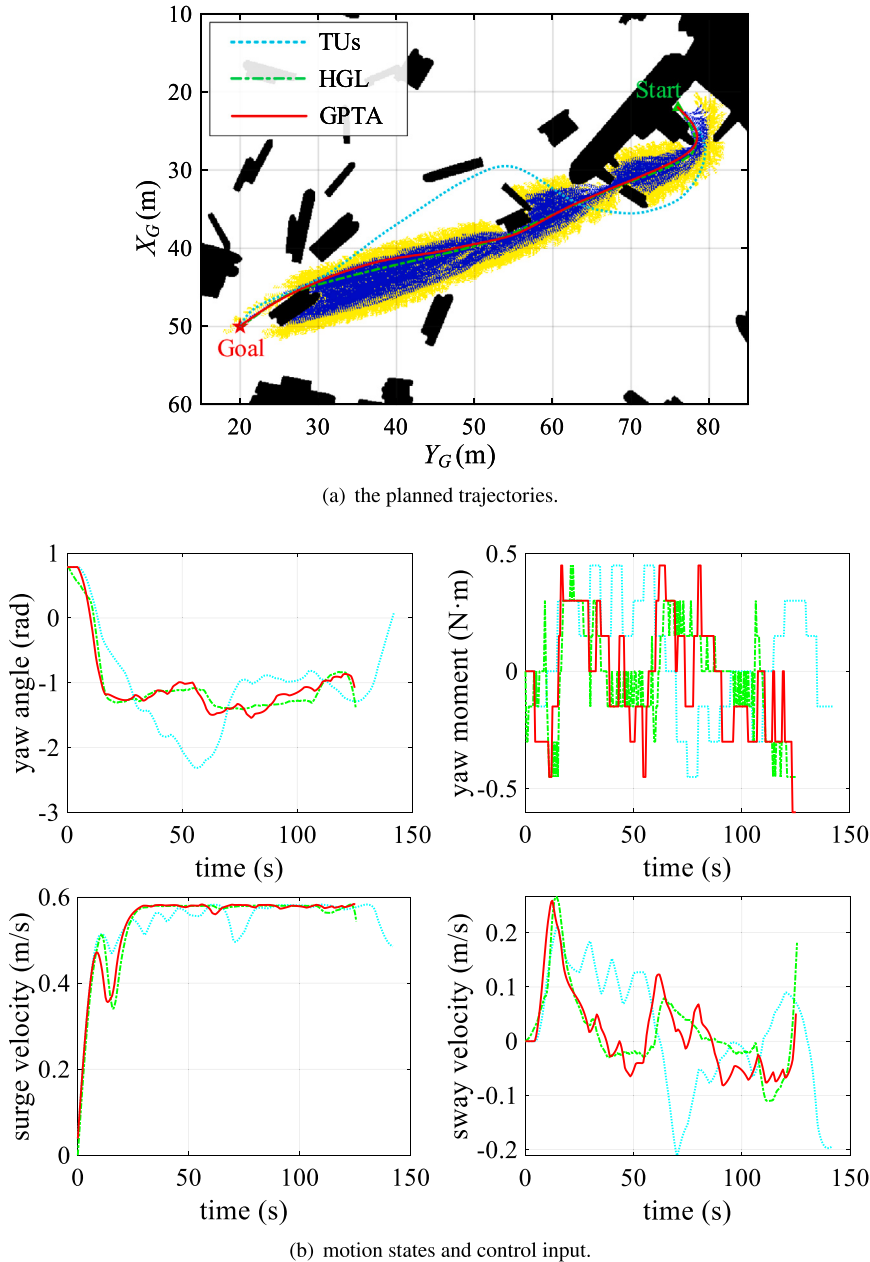


Fig. 9. Comparisons of TU, HGL and GPTA.

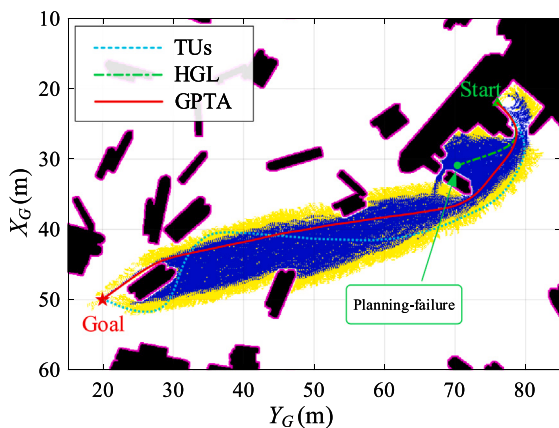


Fig. 10. Trajectories of TU, HGL and GPTA on expanded grid map.

of the accumulated risk value  $\sum R(c)$ , trajectories corresponding to different wind speeds are 7, 8 and 8 respectively. The USV can sail safely.

The performance of GPTA under different wind directions is also discussed. The results of planned trajectories, motion states and yaw moments are shown in Fig. 13. In simulations, the wind speed is fixed as  $V_w = 1.5 \text{ m/s}$ .

It can be seen from Fig. 13(a) that all trajectories obtained by motion planning are relatively similar under different wind directions. The corresponding sailing times of USV are 117.5 s, 120 s and 119 s when the wind directions are  $-\pi/3$ ,  $\pi/3$  and  $\pi$ , respectively. The force component of wind acting on USV increases the sailing speed when the wind direction is  $-\pi/3$ . And the force component of wind acting on the USV reduces its speed and increases the time for arrival when the wind direction is  $\pi$  or  $\pi/3$ . In addition, the accumulated risk values corresponding to different wind directions are 11, 7 and 10 respectively, so all planned trajectories are far away from obstacles. Compared with  $\sum R(c) = 12$  when the wind speed is zero, the impacts of

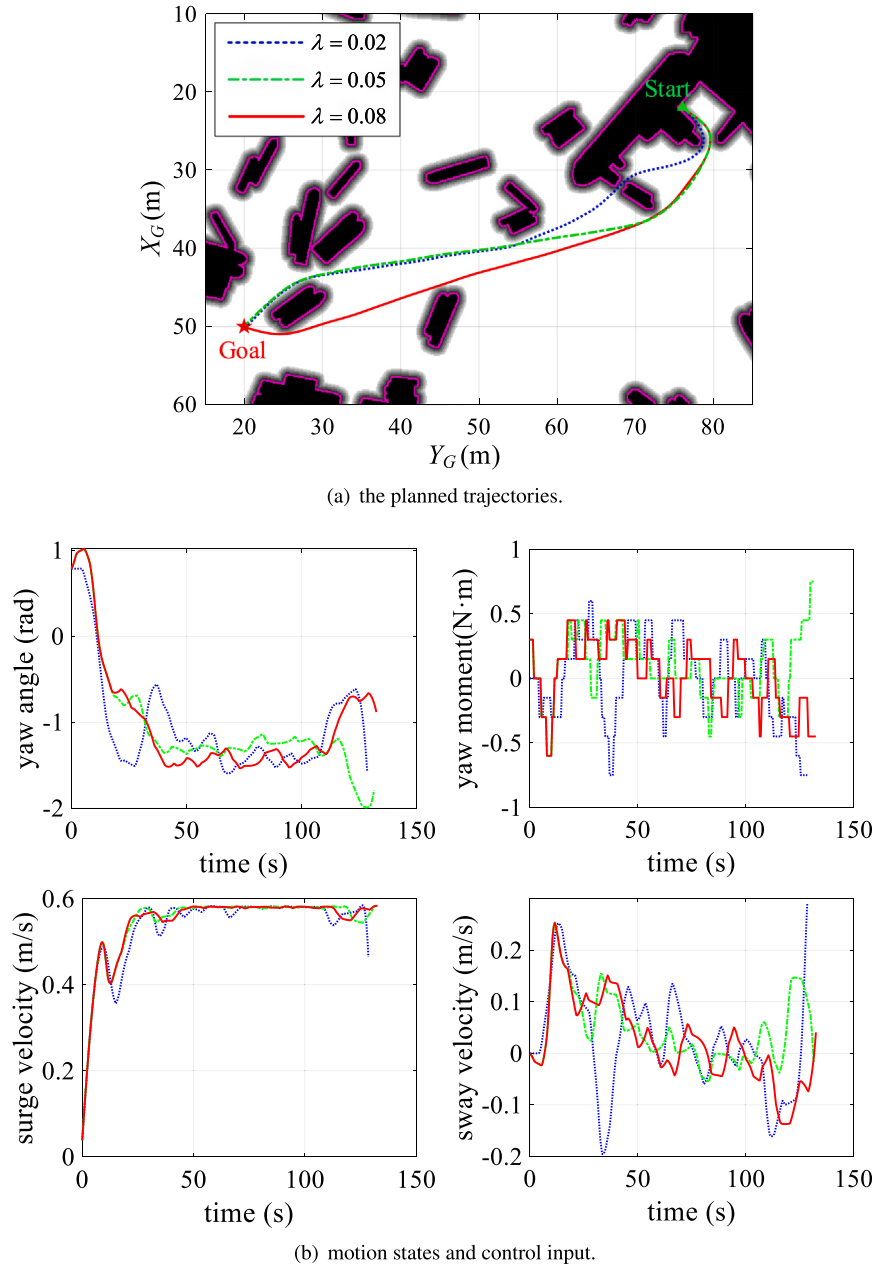


Fig. 11. Comparisons of GPTA with different safety weighting coefficients.

both wind speed and wind direction on the safety of planned trajectory are almost negligible in these simulations.

#### 4.2.2. The influence of current

In present simulations, the initial generalized position of the USV is  $\eta_0 = [33, 10, \pi/2]^T$ , the initial generalized velocity is  $v_0 = [0, 0, 0]^T$ , the goal is  $\eta_g = [33, 86]^T$ , the wind speed is set to 1.5 m/s and wind direction is set to  $\pi$  rad. The current direction of the Yangtze River is fixed at  $\pi/2$  on grid map. The planned trajectories, motion states and yaw moments obtained by using the GPTA under different current speeds are shown in Fig. 14.

When the USV sails downstream, it requires 135.5 s, 130.5 s and 130.5 s to reach the goal under the different current speeds. Normally, the sailing time is proportional to the current speed. However, compared to  $V_c = 0.1$  m/s, the sailing time of the USV does not decrease when the current speed is added to 0.15 m/s. This is because

moving too fast will increase the turning radius of USV. Meanwhile, the trajectory become “tortuous” to avoid obstacles. In addition, the accumulated risk values corresponding to different current speeds are 90, 45 and 72 respectively. Compared with  $\sum R(c) = 14$  when the current speed is zero, sailing downstream will significantly increase the accumulated risk value of planned trajectories. It also indicates that a too large sailing speed will decrease the obstacle avoidance ability of USV.

Under different current speeds, we continue to compare the performance of sailing upstream. The initial generalized position of the USV is changed to  $\eta_0 = [33, 86, -\pi/2]^T$  and the goal is changed to  $\eta_g = [33, 10]^T$ . And the results of planned trajectories, motion states and yaw moments are shown in Fig. 15.

When the USV sails upstream, it takes 154 s, 169 s and 186.5 s to reach the goal under the different current speeds. Correspondingly, the accumulated risk values of the planned trajectories are 31, 20

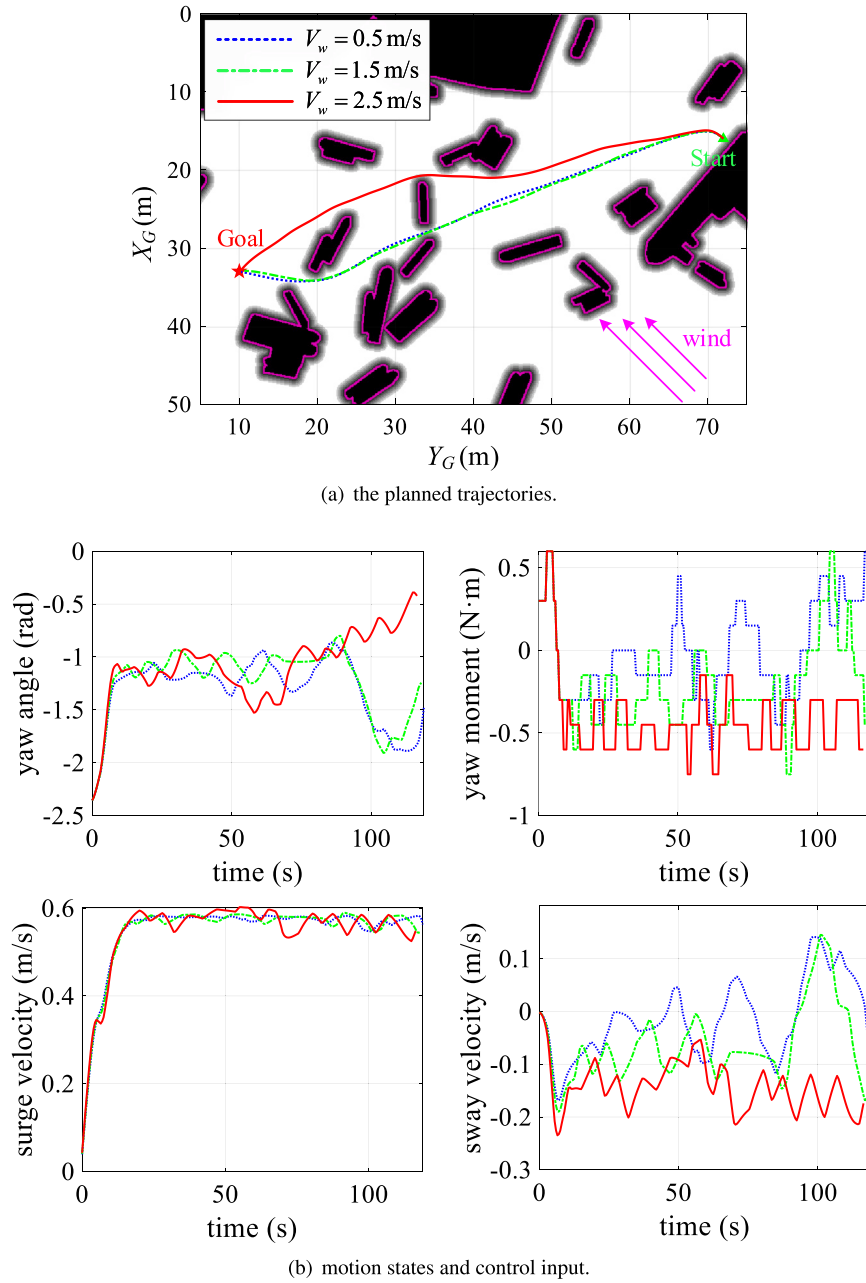


Fig. 12. Influences of different wind speeds.

and 16, respectively. Compared with the tortuous trajectory of sailing downstream, the trajectories obtained in Fig. 15(a) are smooth. In addition, upstream voyage will decrease the relative speed of the USV, the corresponding turning radius will also be reduced, and the ability to avoid obstacles will be enhanced.

#### 4.2.3. Comparisons of HGL and GPTA under the environmental loads

Different from TUs, both HGL and GPTA can take environmental influence into consideration for planning motion. 100 cases are set by selecting different starting points and goal points, as shown in Fig. 16, in which the initial yaw angle is the direction from the starting point to the goal, and the initial generalized velocity is  $v_0 = [0, 0, 0]^T$ . Then, nine different environmental loads are set: the wind direction is fixed at  $\pi$ , and the wind speed is 0.5 m/s, 1.5 m/s, and 2.5 m/s, respectively; the current direction is fixed at  $\pi/2$ , and the current speed is 0.05 m/s, 0.1 m/s, and 0.15 m/s, respectively. The simulations are performed to compare the success rate of planning and sailing time of HGL and

GPTA under different environmental loads, and the results are shown in Table 3. The calculation of sailing time excludes the case where no feasible trajectory can be found by either HGL or GPTA.

According to the data in Table 3, the success rate of GPTA in finding feasible trajectories is much higher than that of HGL, and the average sailing time of planned trajectories is 2.94% faster than HGL. There are 4 cases in total that no feasible trajectory can be found for GPTA, while 25 cases for HGL. Therefore, GPTA is superior to HGL in both success rate of planning and navigation efficiency. The reason why GPTA cannot find the feasible trajectory is that the starting point is too close to the obstacle, which exceed the maneuverability of the underactuated USV. For example, when the starting point is  $[35, 25]^T$  and the goal is  $[35, 31]^T$  in Fig. 16, the USV will not be able to get the feasible trajectory because the starting point is too close to the obstacle. Therefore, the failure to get the feasible trajectory is not caused by the algorithm itself, but by the physical limitations of the USV and the layout of the map.

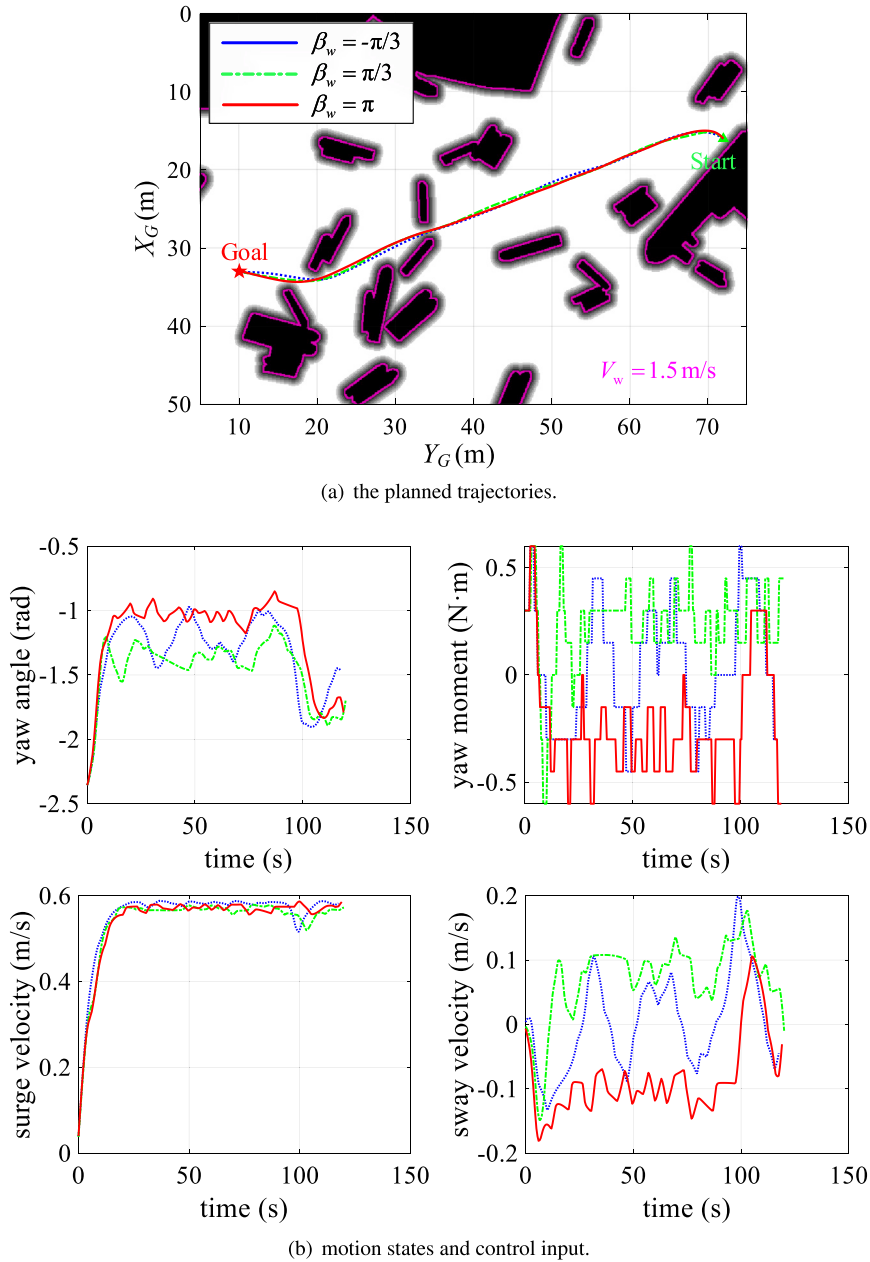


Fig. 13. Influences of different wind directions.

**Table 3**

Performances of HGL and GPTA under different environmental loads.

Environmental impact (m/s)		$V_w = 0.5$ $V_c = 0.05$	$V_w = 0.5$ $V_c = 0.1$	$V_w = 0.5$ $V_c = 0.15$	$V_w = 1.5$ $V_c = 0.05$	$V_w = 1.5$ $V_c = 0.1$	$V_w = 1.5$ $V_c = 0.15$	$V_w = 2.5$ $V_c = 0.05$	$V_w = 2.5$ $V_c = 0.1$	$V_w = 2.5$ $V_c = 0.15$
Success rate	HGL	84%	83%	84%	80%	84%	81%	82%	80%	82%
	GPTA	99%	98%	96%	100%	99%	96%	100%	100%	100%
Sailing time (s)	HGL	68	72.78	78.64	68.37	71.35	75.12	67.54	69.79	74.55
	GPTA	67.79	72.57	78.46	67.92	71.10	75.23	67.36	69.83	73.98

## 5. Conclusion

In this paper, two global motion planning approaches, PTA and GPTA, are proposed to find a high-efficiency trajectory considering all dynamic constraints of the underactuated USV. PTA and GPTA integrate predicted trajectories directly into the grid map and search the final trajectory by A\* search method with consideration of efficiency and safety. In order to verify the efficacy of the proposed approaches,

multiple numerical experiments with different methods and environmental perturbations are implemented and relevant conclusions are summarized as follows:

- (1) Different from PTA using Euclidean distance directly, GPTA has a better estimate for the heuristic cost of the objective function through a global path obtained by Theta\*. Therefore, GPTA is superior to PTA in terms of both computational efficiency and navigation efficiency.

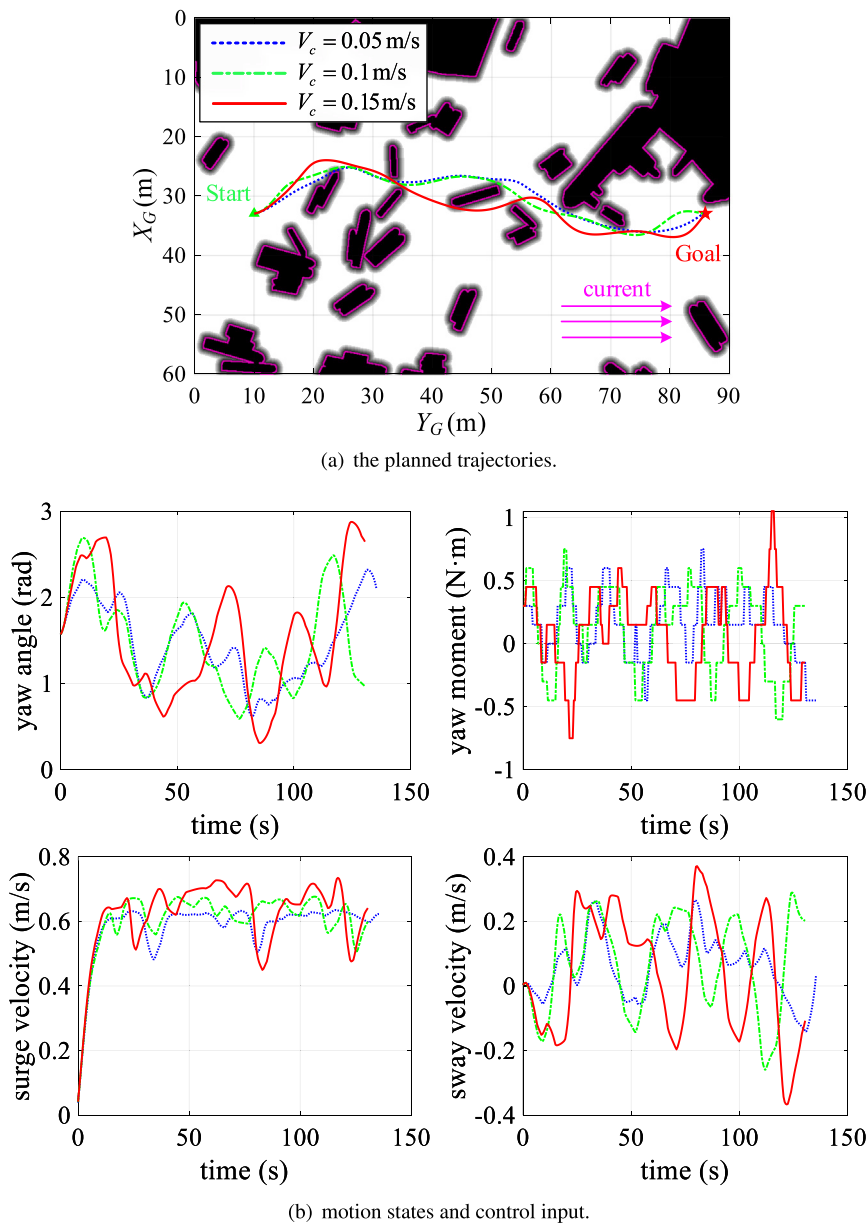


**Fig. 14.** Comparisons of GPTA with different current speeds when the USV sails downstream.

- (2) Compared to TUs and HGL, GPTA can find a more efficient trajectory on both unexpanded and expanded grid maps. In terms of success rate of planning, GPTA also has better performance, especially in narrow waters.
- (3) PTA and GPTA proposed in present paper can take environmental factors into account. In a complex terrain like the anchorage used in present paper, the planned trajectories of USV sailing downstream are more tortuous and dangerous than sailing upstream by comparing their voyage and accumulated risk values.

GPTA usually takes ten or even tens of seconds to find the efficient trajectory. Although the global motion planning can ignore the real-time performance, it is an indisputable fact that the computational efficiency of GPTA is relatively poor. The algorithm will be improved to increase computational efficiency in the future.

#### CRediT authorship contribution statement

**Sen Han:** Conceptualization, Methodology, Software, Data curation, Investigation, Writing - original draft, Writing - review & editing,

**Visualization.** **Lei Wang:** Conceptualization, Methodology, Software, Investigation, Writing - review & editing. **Yiting Wang:** Methodology, Investigation, Supervision, Project administration, Funding acquisition. **Huacheng He:** Methodology, Software, Investigation, Writing - review & editing, Visualization.

#### Declaration of competing interest

The authors declare that they have no known competing financial interests or personal relationships that could have appeared to influence the work reported in this paper.

#### Acknowledgments

The authors greatly acknowledge the support of the National Natural Science Foundation of China (Grant No. 51179103), the Ministry of Industry and Information Technology, China (Grant No. [2018] 473) and the Hainan Provincial Joint Project of Sanya Bay Science and Technology City, China (Grant No. 520LH051).

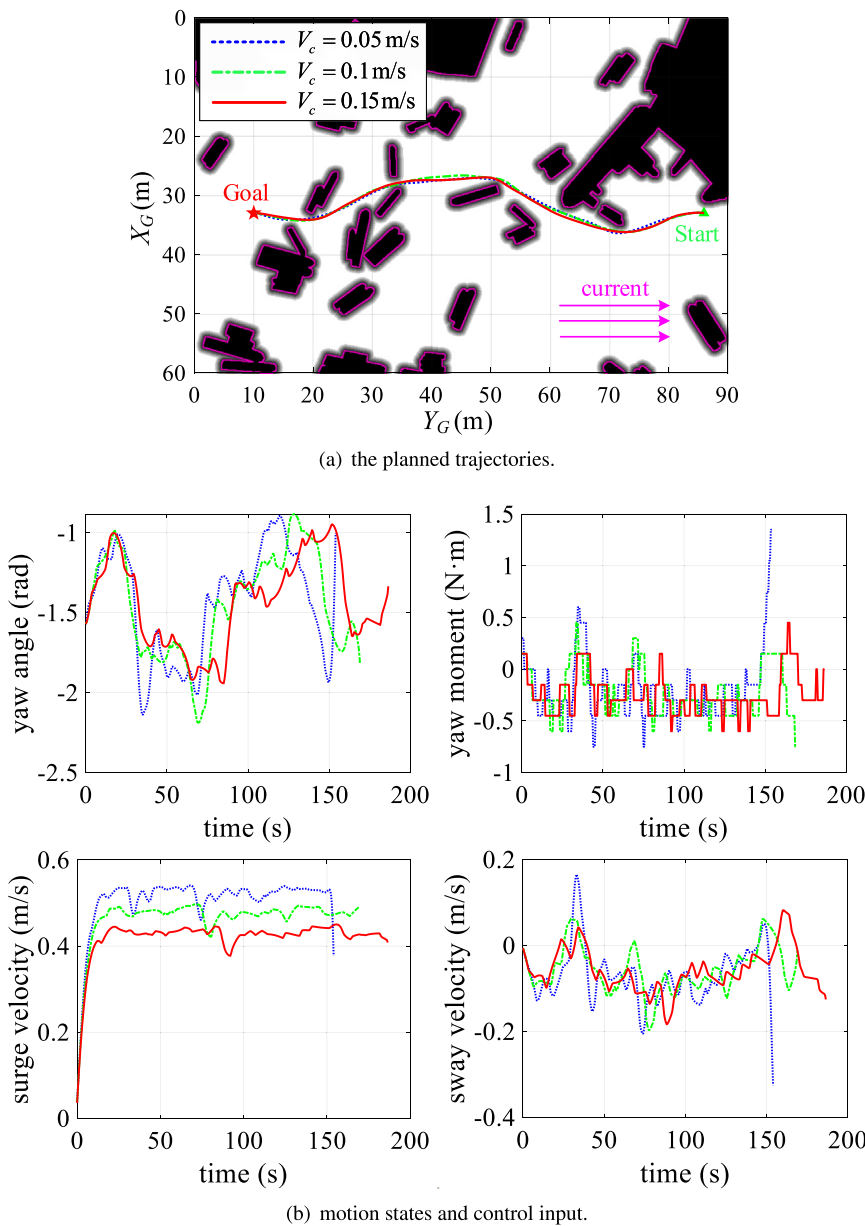


**Fig. 15.** Comparisons of GPTA with different current speeds when the USV sails upstream.

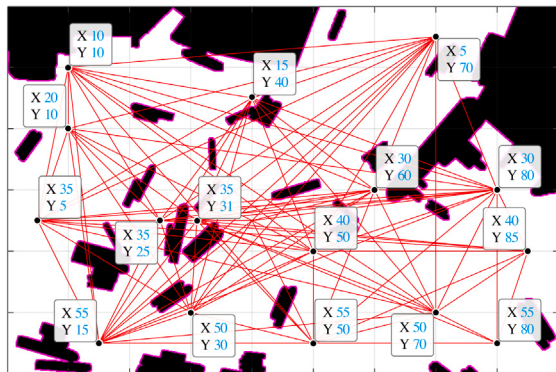


**Fig. 16.** The setting cases of different starting points and goal points.

## References

- Bertaska, I.R., Alvarez, J., Sinisterra, A., von Ellenrieder, K., Dhanak, M., Shah, B., Švec, P., Gupta, S.K., 2013. Experimental evaluation of approach behavior for autonomous surface vehicles. In: ASME 2013 Dynamic Systems and Control Conference, Palo Alto, California, USA.
- Bertaska, I.R., von Ellenrieder, K.D., 2019. Experimental evaluation of supervisory switching control for unmanned surface vehicles. *IEEE J. Ocean. Eng.* 44 (1), 7–28.
- Bertaska, I.R., Shah, B., von Ellenrieder, K., Švec, P., Klinger, W., Sinisterra, A.J., Dhanak, M., Gupta, S.K., 2015. Experimental evaluation of automatically-generated behaviors for USV operations. *Ocean Eng.* 106, 496–514.
- Chen, P., Huang, Y., Papadimitriou, E., Mou, J., van Gelder, P., 2020. Global path planning for autonomous ship: A hybrid approach of fast marching square and velocity obstacles methods. *Ocean Eng.* 214, 107793.
- Chen, Z., Zhang, Y., Zhang, Y., Nie, Y., Tang, J., Zhu, S., 2019. A hybrid path planning algorithm for unmanned surface vehicles in complex environment with dynamic obstacles. *IEEE Access* 7, 126439–126449.
- Chrpa, L., Osborne, H., 2014. Towards a trajectory planning concept: augmenting path planning methods by considering speed limit constraints. *J. Intell. Robot. Syst.* 75 (2), 243–270.
- Claussmann, L., Revilloud, M., Gruyer, D., Glaser, S., 2020. A review of motion planning for highway autonomous driving. *IEEE Trans. Intell. Transp. Syst.* 21 (5), 1826–1848.

- Daniel, K., Nash, A., Koenig, S., Felner, A., 2010. Theta\*: Any-angle path planning on grids. *J. Artificial Intelligence Res.* 39, 533–579.
- Dolgov, D., Thrun, S., Montemerlo, M., Diebel, J., 2010. Path planning for autonomous vehicles in unknown semi-structured environments. *Int. J. Robot. Res.* 29 (5), 485–501.
- Du, Z., Wen, Y., Xiao, C., Huang, L., Zhou, C., Zhang, F., 2019. Trajectory-cell based method for the unmanned surface vehicle motion planning. *Appl. Ocean Res.* 86, 207–221.
- Du, Z., Wen, Y., Xiao, C., Zhang, F., Huang, L., Zhou, C., 2018. Motion planning for unmanned surface vehicle based on trajectory unit. *Ocean Eng.* 151, 46–56.
- Fossen, T.I., 2011. *Handbook of Marine Craft Hydrodynamics and Motion Control*. John Wiley & Sons.
- Fossen, T., Pettersen, K.Y., Nijmeijer, H., 2017. *Sensing and Control for Autonomous Vehicles*. Springer.
- Gu, S., Zhou, C., Wen, Y., Zhong, X., Zhu, M., Xiao, C., Du, Z., 2020. A motion planning method for unmanned surface vehicle in restricted waters. *Proc. Inst. Mech. Eng. M* 234 (2), 332–345.
- Han, S., Wang, Y., Wang, L., He, H., 2021. Automatic berthing for an underactuated unmanned surface vehicle: A real-time motion planning approach. *Ocean Eng.* 235, 109352.
- Hart, P.E., Nilsson, N.J., Raphael, B., 1968. A formal basis for the heuristic determination of minimum cost paths. *IEEE Trans. Syst. Sci. Cybern.* 4 (2), 100–107.
- Karaman, S., Frazzoli, E., 2010. Incremental sampling-based algorithms for optimal motion planning. In: *Robotics: Science and Systems 2010*, Zaragoza, SPAIN.
- Kim, H., Kim, D., Shin, J.-U., Kim, H., Myung, H., 2014. Angular rate-constrained path planning algorithm for unmanned surface vehicles. *Ocean Eng.* 84, 37–44.
- Lee, T.-K., Baek, S.-H., Choi, Y.-H., Oh, S.-Y., 2011. Smooth coverage path planning and control of mobile robots based on high-resolution grid map representation. *Robot. Auton. Syst.* 59 (10), 801–812.
- Lee, T., Kim, H., Chung, H., Bang, Y., Myung, H., 2015. Energy efficient path planning for a marine surface vehicle considering heading angle. *Ocean Eng.* 107, 118–131.
- Li, Y., Cui, R., Li, Z., Xu, D., 2018. Neural network approximation based near-optimal motion planning with kinodynamic constraints using RRT. *IEEE Trans. Ind. Electron.* 65 (11), 8718–8729.
- Likhachev, M., Ferguson, D., 2009. Planning long dynamically feasible maneuvers for autonomous vehicles. *Int. J. Robot. Res.* 28 (8), 933–945.
- Liu, Y., Bucknall, R., 2016. The angle guidance path planning algorithms for unmanned surface vehicle formations by using the fast marching method. *Appl. Ocean Res.* 59, 327–344.
- Liu, Y., Bucknall, R., Zhang, X., 2017. The fast marching method based intelligent navigation of an unmanned surface vehicle. *Ocean Eng.* 142, 363–376.
- Lozano-Pérez, T., Wesley, M.A., 1979. An algorithm for planning collision-free paths among polyhedral obstacles. *Commun. ACM* 22 (10), 560–570.
- Moon, C.-b., Chung, W., 2015. Kinodynamic planner dual-tree RRT (DT-RRT) for two-wheeled mobile robots using the rapidly exploring random tree. *IEEE Trans. Ind. Electron.* 62 (2), 1080–1090.
- Nash, A., Koenig, S., 2013. Any-angle path planning. *AI Mag.* 34 (4), 85–107.
- Niu, H., Ji, Z., Savvaris, A., Tsourdos, A., 2020. Energy efficient path planning for unmanned surface vehicle in spatially-temporally variant environment. *Ocean Eng.* 196, 106766.
- Niu, H., Lu, Y., Savvaris, A., Tsourdos, A., 2018. An energy-efficient path planning algorithm for unmanned surface vehicles. *Ocean Eng.* 161, 308–321.
- Petti, S., Fraichard, T., 2005. Safe motion planning in dynamic environments. In: *2005 IEEE/RSJ International Conference on Intelligent Robots and Systems*, Edmonton, CANADA, pp. 2210–2215.
- Salzman, O., Halperin, D., 2016. Asymptotically near-optimal RRT for fast, high-quality motion planning. *IEEE Trans. Robot.* 32 (3), 473–483.
- Shah, B., Gupta, S., 2016. Speeding up A\* search on visibility graphs defined over quadtrees to enable long distance path planning for unmanned surface vehicles. In: *Proceedings of the International Conference on Automated Planning and Scheduling*, vol. 26, no. 1, pp. 527–535.
- Shah, B.C., Gupta, S.K., 2019. Long-distance path planning for unmanned surface vehicles in complex marine environment. *IEEE J. Ocean. Eng.* 45 (3), 813–830.
- Shah, B.C., Švec, P., Bertaska, I.R., Sinisterra, A.J., Klinger, W., von Ellenrieder, K., Dhanak, M., Gupta, S.K., 2016. Resolution-adaptive risk-aware trajectory planning for surface vehicles operating in congested civilian traffic. *Auton. Robot.* 40 (7), 1139–1163.
- Sharma, S.K., Sutton, R., Motwani, A., Annamalai, A., 2014. Non-linear control algorithms for an unmanned surface vehicle. *Proc. Inst. Mech. Eng. M* 228 (2), 146–155.
- Shi, B., Su, Y., Wang, C., Wan, L., Luo, Y., 2019. Study on intelligent collision avoidance and recovery path planning system for the waterjet-propelled unmanned surface vehicle. *Ocean Eng.* 182, 489–498.
- Skjetne, R., Smogeli, Ø.N., Fossen, T.I., 2004. A nonlinear ship manoeuvring model: Identification and adaptive control with experiments for a model ship. *Model. Identif. Control* 25 (1), 3–27.
- Song, R., Liu, Y., Bucknall, R., 2019. Smoothed A\* algorithm for practical unmanned surface vehicle path planning. *Appl. Ocean Res.* 83, 9–20.
- Švec, P., Gupta, S.K., 2012. Automated synthesis of action selection policies for unmanned vehicles operating in adverse environments. *Auton. Robot.* 32 (2), 149–164.
- Švec, P., Shah, B.C., Bertaska, I.R., Alvarez, J., Sinisterra, A.J., Von Ellenrieder, K., Dhanak, M., Gupta, S.K., 2013. Dynamics-aware target following for an autonomous surface vehicle operating under COLREGs in civilian traffic. In: *2013 IEEE/RSJ International Conference on Intelligent Robots and Systems*, Tokyo, JAPAN, pp. 3871–3878.
- Švec, P., Thakur, A., Raboin, E., Shah, B.C., Gupta, S.K., 2014. Target following with motion prediction for unmanned surface vehicle operating in cluttered environments. *Auton. Robot.* 36 (4), 383–405.
- Wang, N., Gao, Y., Zheng, Z., Zhao, H., Yin, J., 2018. A hybrid path-planning scheme for an unmanned surface vehicle. In: *2018 Eighth International Conference on Information Science and Technology*, Cordoba, SPAIN, pp. 231–236.
- Wang, N., Jin, X., Er, M.J., 2019. A multilayer path planner for a USV under complex marine environments. *Ocean Eng.* 184, 1–10.
- Wang, N., Xu, H., 2020. Dynamics-constrained global-local hybrid path planning of an autonomous surface vehicle. *IEEE Trans. Veh. Technol.* 69 (7), 6928–6942.
- Wang, N., Xu, H., Li, C., Yin, J., 2020. Hierarchical path planning of unmanned surface vehicles: A fuzzy artificial potential field approach. *Int. J. Fuzzy Syst.* 1–12.
- Wu, G., Atilla, I., Tahsin, T., Terziev, M., Wang, L., 2021. Long-voyage route planning method based on multi-scale visibility graph for autonomous ships. *Ocean Eng.* 219, 108242.
- Yoo, B., Kim, J., 2016. Path optimization for marine vehicles in ocean currents using reinforcement learning. *J. Mar. Sci. Technol.* 21 (2), 334–343.
- Zhang, F., Marani, G., Smith, R.N., Choi, H.T., 2015. Future trends in marine robotics. *IEEE Robot. Autom. Mag.* 22 (1), 14–122.
- Zhong, X., Tian, J., Hu, H., Peng, X., 2020. Hybrid path planning based on safe A\* algorithm and adaptive window approach for mobile robot in large-scale dynamic environment. *J. Intell. Robot. Syst.* 99 (1), 65–77.
- Zhou, C., Gu, S., Wen, Y., Du, Z., Xiao, C., Huang, L., Zhu, M., 2020a. Motion planning for an unmanned surface vehicle based on topological position maps. *Ocean Eng.* 198, 106798.
- Zhou, C., Gu, S., Wen, Y., Du, Z., Xiao, C., Huang, L., Zhu, M., 2020b. The review unmanned surface vehicle path planning: Based on multi-modality constraint. *Ocean Eng.* 200, 107043.